Generation of Acoustic Disturbances in Supersonic Laminar Cavity Flows

Weipeng Li

Dept. of Aeronautics and Astronautics, Shanghai Jiaotong University, Shanghai, 200-240, China

Taku Nonomura and Kozo Fujii

Institute of Space and Astronautics Science/JAXA, Sagamihara, Kanagawa, 252-5210, Japan

The generation of acoustic disturbances in supersonic laminar cavity flows is investigated by large-eddy simulations of supersonic laminar flow ($M = 1.2, 2.0,$ and 3.0) past a rectangular cavity with a length-to-depth ratio of 2. Results suggest that well-originated large-scale vortical structures with strong spanwise coherence are present in the shear layer. Compressibility effects have significant impacts on the shear-layer development and the fluctuation properties. The dominant mechanism for the acoustic radiation in supersonic laminar cavity flows is shown to be associated with the successive passage of large-scale vortices over the cavity trailing edge. It is found that Mach waves radiated from the cavity shear layer may have significant contributions for the noiseradiation in terms of enhancing the strength of the feedback compression waves.

1. INTRODUCTION

Supersonic flow past cavities has been studied for many years, both in practical and academic interest. In general, when the length-to-depth ratio (L/D) of a rectangular cavity is less than ten, the shear layer reattaches on the cavity aft wall. This type of cavity flow is termed open cavity flow.[1,2] An undesirable problem in open cavity flow is the existence of intense resonant noise. For instance, a resonance with a sound pressure level of 160 decibels is observed in a cavity flow at Mach number 2.0.[3] The resonant noise may harm the nearby equipment and the environment, for example, by causing structural vibrations and fatigue, adverse effects on store separation, and undesirable noise.

Reviews of cavity flows were conducted by Grace, Colonius, Rockwell and Naudascher,[4] and Lawson and Barakos.[5] The driving mechanism of cavity oscillations is widely regarded as a feedback mechanism between shear-layer instabilities and acoustic disturbances. It was first proposed by Powell for the study of edge tones.[6] In 1964, Rossiter developed a semi-empirical formula to predict the resonance frequencies based on his extensive experimental data with freestream Mach number within the range of 0.5 and 1.2.[7] Heller et al. improved Rossiters formula by introducing a temperature recover factor.[8] A typical feedback cycle consists of four key procedures: (1) the shear layer near the leading edge of the cavity is excited by acoustic disturbances, which leads to the generation of discrete vortices; (2) the vortices grow large as they convect downstream and eventually impact on the cavity trailing edge; (3) feedback compression waves (upstream-traveling) are radiated near the cavity trailing edge; and (4) the feedback compression waves propagate upstream and excite the shear layer again. Then, the feedback cycle is closed.

Despite the fact that the feedback mechanism itself has been well established and accepted, the mechanism driving the self-sustained oscillations in supersonic cavity flows is still not precisely resolved. One of the most important factors is the generation of acoustic disturbances near the downstream cavity lip. Rossiter observed that discrete vortices are shed periodically from the leading edge of the cavity and convect downstream until they encounter the downstream cavity lip.[7] He assumed that the passage of vortices over the trailing edge is responsible for the acoustic radiation. Heller and Bliss emphasized that discrete vortices were not usually observed in their experiment with a Mach number varying from 0.8 to 2.0.[9] They stated that the generation of acoustic disturbances is caused by the periodic mass addition and removal near the cavity trailing edge. Zhang reported that the compression wave emission is related to the shear layer deflection, which, in turn, is associated with the vortex production and convection.[10] By description of an oscillation cycle, Tam et al. stated that the upstream-travelling compression wave is generated by a pressure wave reflection at the bottom aft wall.[11] An experimental study by Schmit et al. showed that the entrained waves are the start of the feedback loop process rather than the shear layer impingement on the downstream cavity wall, as many references have indicated.[12] Supersonic laminar flow past cavities usually exists over the orbiter launch/reentry trajectories; however, limited investigations have been conducted. Krishnamurty experimentally observed that the laminar cavity flow produced louder resonant noise than that of turbulent cavity flow.[13] Heller et al. reported that no resonance was observed in the turbulent cavity flow at Ma3.0; however, a strong resonant peak occurred in the laminar cavity flow.[14] Based on large-eddy simulations of high subsonic laminar cavity flow, Gloerfelt et al. stated that the strong unsteadiness of the internal recirculation flow can be associated with the possible vortex coalescence.[15] The physical mechanisms underlying the self-sustained oscillations in supersonic laminar cavity flows are in need of more study, especially on the generation of acoustic disturbances.

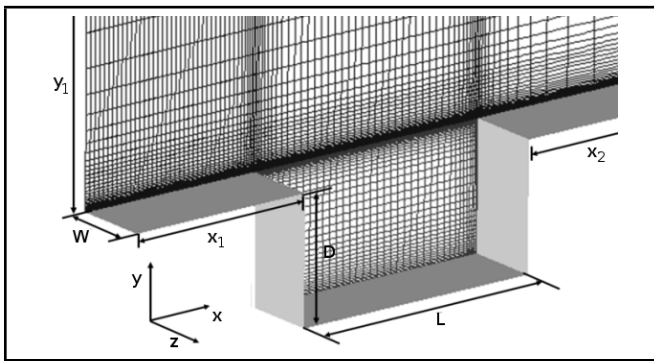This paper aims to address the generation mechanism of

Figure 1. Computational grids (shown every other five points).

Figure 2. Distributions of time-averaged streamwise velocities.

Figure 3. Distributions of root-mean-square of pressure fluctuations along the internal cavity walls.

acoustic disturbances in supersonic laminar cavity flows. An introduction of numerical methods is given in Section 2. In Section 3, we describe the features of flow fields with an increase of the freestream Mach number. In Section 4, the generation of acoustic disturbance in the vicinity of the downstream cavity lip is investigated. This paper will be concluded in Section 5.

2. NUMERICAL METHODS

2.1. Flow Conditions

Supersonic flows past a cavity of $L/D = 2$, $W/D = 0.6$ were numerically studied, where L is the length of the cavity, W is the width of the cavity, and D was the depth of the cavity. Three simulations were conducted with freestream Mach numbers of 1.2, 2.0, and 3.0. The Reynolds number based on the cavity depth was set to 10^5. The reference velocity was set as the sound speed. The boundary layer thickness δ_0 was $0.075D$.

2.2. Numerical Methods

The governing equations were three-dimensional compressible Navier-Strokes equations in conservative form. Implicit large-eddy simulations (ILES) were conducted, which rely on numerical dissipation to dissipate high-frequency turbulent energy. In order to meet the low-dispersive and low-dissipative requirements of computational aeroacoustics (CAA), a modified seventh-order weighted compact nonlinear scheme (WCNS) was employed for spatial derivatives.[16–18] The numerical fluxes were evaluated by the simple high-resolution upwind scheme (SHUS) which was a family of advection-upstream-splitting-method (AUSM) type schemes.[19] Viscous terms were evaluated by a sixth-order central difference scheme. Alternate directional implicit symmetric Gauss-Seidel (ADI-SGS) scheme was applied for time integration.[20] A second-order temporal accuracy is obtained using three Newton-like sub-iterations. The CFL number was equal to 1.2.

The computational domain consisted of inside cavity region and upper cavity region, as shown in Fig. 1. Structured grids were adopted, and the total grid points were about 7.0 million. The grid had 200×169×80 points inside the cavity and 360×150×80 points in the region above the cavity. The origin of the coordinate system was located at the middle of the leading-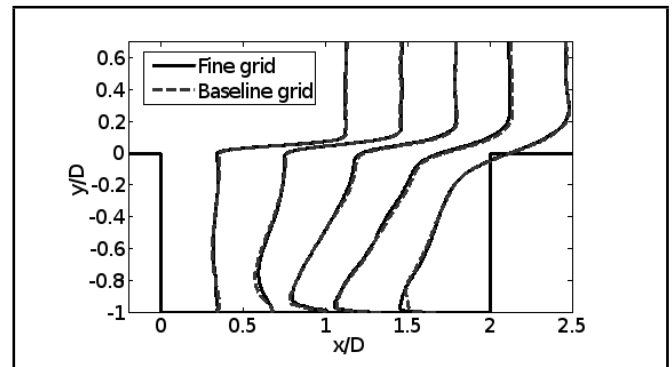edge lip. The length from the inflow boundary to the leading edge x_1 was equal to $1.5D$, and a length of $x_2 = 4D$ was extended from the trailing edge to the outflow boundary. A length of $4D$ was extended in the vertical direction, and no buffer region was set because of supersonic freestream. The grid spacing was refined in the near-wall regions. The minimum and maximum grid spacing was $0.0005D$ and $0.012D$, respectively. The Blasius profile was imposed for the initial inflow. No-slip adiabatic wall boundary condition is imposed for all wall boundaries. Zero-gradient pressure condition was employed at the outflow and upper boundary. Periodic boundary condition was given in the spanwise direction.
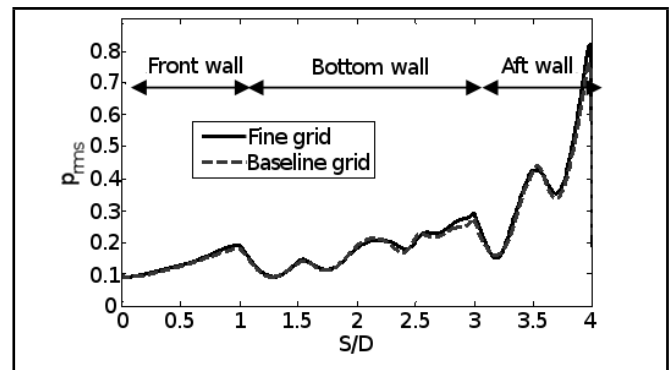
2.3. Validations

The baseline grid was refined by a factor of 1.333 in each direction for a validation of grid convergence. The fine grid contains 18.3 million grid points in total. Flow conditions were the same as those in the Ma2.0 case. Figure 2 shows the distributions of the time-averaged streamwise velocities. It indicates that the simulation with the baseline grid had almost the same velocity profiles as that with the fine grid. Figure 3 shows the distributions of root-mean-square of pressure fluctuations p_{rms} along the internal cavity walls. Apparently, a fairly good agreement is calculated between the two simulations.

Figure 4 shows the pressure spectra at the mid-point of the cavity front wall (P_1). The sound pressure level (SPL) was defined by $SPL = 20log_{10}(p/p_{ref})$, where $p_{ref} = 2.0 \times 10^{-5}[Pa] \times p_\infty$. The standard Strouhal number St was defined by $St = fL/U_\infty$, where f is frequency and U_∞ is freestream velocity. The resonance frequencies observed with the baseline grid and fine grid agree well with each other and also match with the experimental study of Zhuang et al.
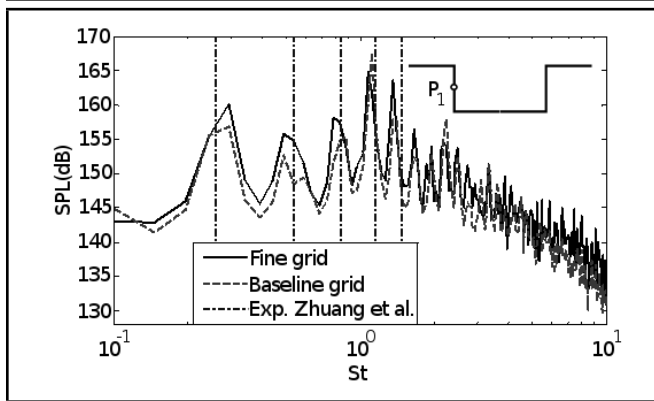
Figure 4. Pressure spectra at the mid-point of the cavity front wall.

$(M_\infty = 2.0, ReD = 5.4 \times 10^5$, turbulent inflow).[21] The differences in the SPL amplitude do not influence our conclusions since the objective of this paper is to address the fundamental physics rather than to accurately predict the cavity tones. The following simulations are conducted with the baseline grid.

3. FLOW FIELDS

Snapshots of instantaneous flow fields are shown in Fig. 5. Large-scale vortical structures with strong spanwise coherence are present in the cavity shear layer. They convect downstream with their own trajectories and speeds. Plenty of small-scale vortical structures are observed in the shear-layer region as well as the internal recirculation region. It shows a good turbulence resolution with the high-order numerical schemes. It is noted that, in our preliminary two-dimensional simulations, the cavity shear layer consisted of much larger size of vortical structures, and behaves more violently than that in these three-dimensional simulations.

Figure 6 shows the variation of vorticity thickness between cavity lips, and its slope was used to measure the shear-layer growth rate. Dashed lines are used to indicate linear shear-layer growth rates. Basically, the growth of the cavity shear layer is similar to that of free shear layers. After the upstream boundary layer separated from the leading edge, the cavity shear layer started to grow due to the Kelvin-Helmholtz instabilities. In this region, the cavity shear layer was dominated by a transition procedure from laminar inflow to turbulence, and a slow shear-layer growth rate appeared near the cavity leading edge which is quite different from that in turbulent cavities.[22] This transition procedure was impacted by compressibility effects, that is, higher-speed inflow corresponds to a longer distance to complete this transition procedure. In the Ma3.0 case, the shear-layer growth rate remains at low values across the cavity lips, and it seems that the transition procedure does not complete within the cavity length. However, in the Ma1.2 and Ma2.0 cases, the shear-layer growth rate resumed a standard value after the transition procedure, indicating that the cavity shear layer grows linearly and obeys a self-similarity rule which can always be observed in free shear layers. Three-dimensional characteristics are dominant in this region. Near the cavity trailing edge, the shear-layer growth rate drops quickly because of the distortion of the mean velocity.

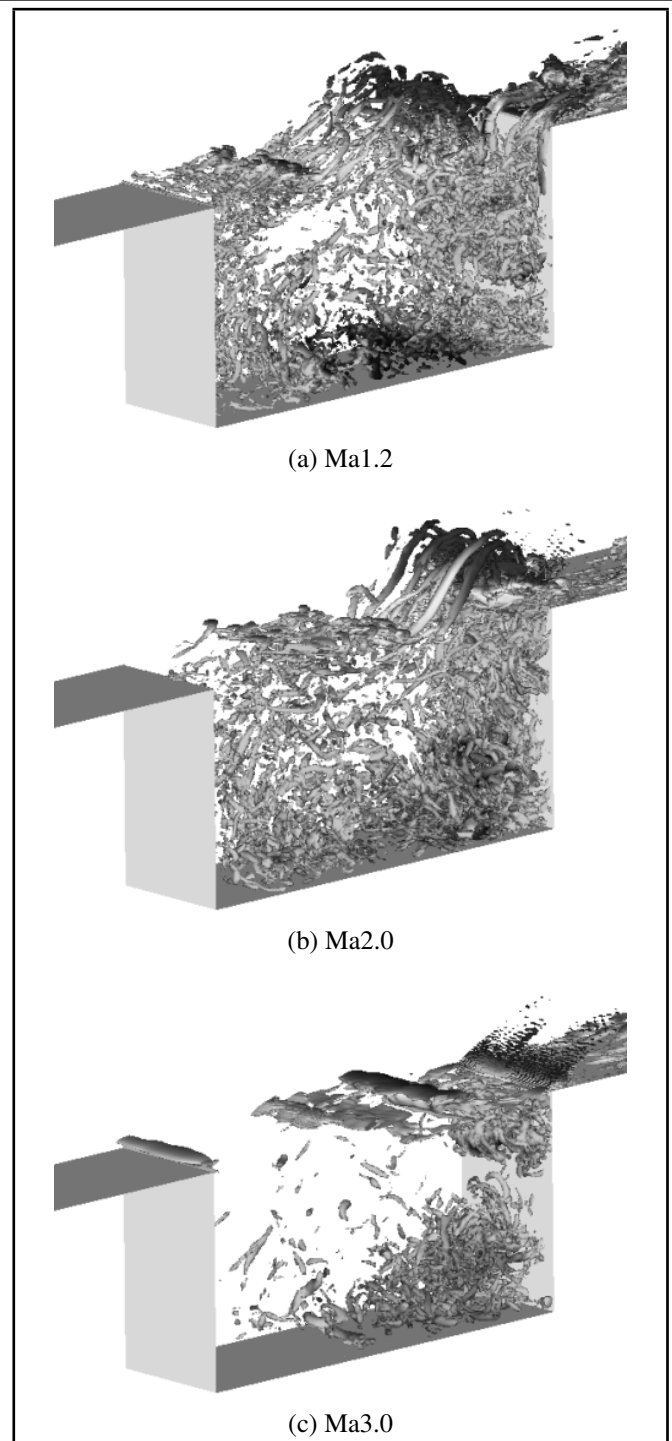Two differences may exist between the cavity shear layer

(a) Ma1.2

(b) Ma2.0

(c) Ma3.0

Figure 5. Snapshots of instantaneous flow-fields. Iso-surface of the second invariant of velocity gradient tensors, $Q_{2nd} = 50(a_\infty/D)^2$; colored with streamwise velocity, $-0.5 < u/u_\infty < 1$.

and free shear layers: (1) the cavity shear layer is subjected to strong acoustic disturbances, which lead to strong spanwise coherent vortices near the leading edge. However, the free shear layers at supersonic speed are generally dominated by oblique modes, (2) the interactions between the cavity shear layer and recirculation flows cannot be omitted in the supersonic cavity flows since high-speed recirculation flow exists inside the cavity.[23]

In order to assess the fluctuation properties, contours of turbulence kinetic energy (TKE) were plotted in Fig. 7. Great velocity distortions and deformations are generated near the
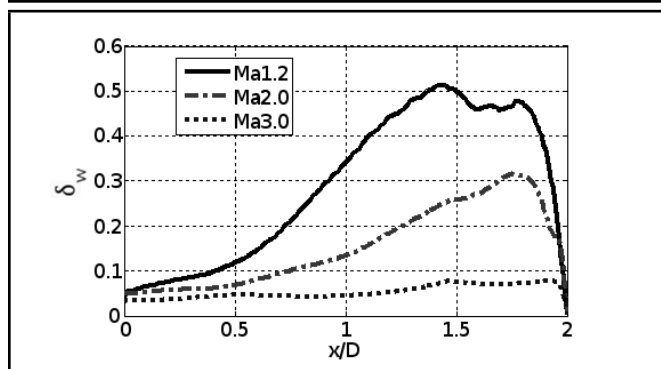
Figure 6. Variations of vorticity shear-layer thickness.

cavity trailing edge due to the impingement of the shear layer, corresponding high values of TKE near the cavity trailing edge. The distribution of TKE in the Ma1.2 case has broad distributions in the vertical direction, while the fluctuations in the Ma3.0 case are mostly constrained in a thin layer. This result may be associated with the compressibility effects of high-speed flows.

4. GENERATION OF ACOUSTIC DISTURBANCES

In our previous work, the mechanism driving supersonic laminar cavity oscillations has been verified to be a feed-back mechanism between discrete vortices and acoustic disturbances.[24] The acoustic disturbances in terms of feedback (upstream-travelling) compression waves were radiated from the region near the cavity trailing edge. But their generation mechanism was discussed less. In the present study, we attempt to demonstrate that the generation of acoustic disturbances is highly associated with two mechanisms: the successive passage of large-scale vortices over the trailing edge and the reflection of Mach waves. A schematic of large-scale vortices and Mach waves is plotted in Fig. 8. In the Ma2.0 and Ma3.0 cases, the large-scale vortices convect at supersonic speed, and intense Mach waves propagate with the large-scale vortices; in the Ma1.2 case, no Mach wave is radiated from the cavity shear layer since the convection velocity of large-scale vortices is at subsonic speed.[24]

4.1. The Passage of Large-scale Vortices over the Trailing Edge

Rossiter assumed that the passage of large-scale vortices over the cavity trailing edge was responsible for the acoustic radiation, but no quantitative discussion was given.[7] Here, we attempt to provide more quantitative evidence by use of a phase-averaging analysis.[25]

Figure 9 shows the convection trajectories of vortex cores from the leading edge to the trailing edge of the cavity. The vortex cores are marked by detecting the maximum value of Q criterionin the phase-averaged flow fields.[24] The upstream boundary-layer rolls up into two well-originated vortices (S_1 and S_2) in phases of each acoustic excitation. Vortex pairing occurs in the Ma1.2 case. Based on our animations and vortex trajectories in $x - y$ axes, the vortex S_1 goes inside the cavity and is not critical for the generation of acoustic disturbances.
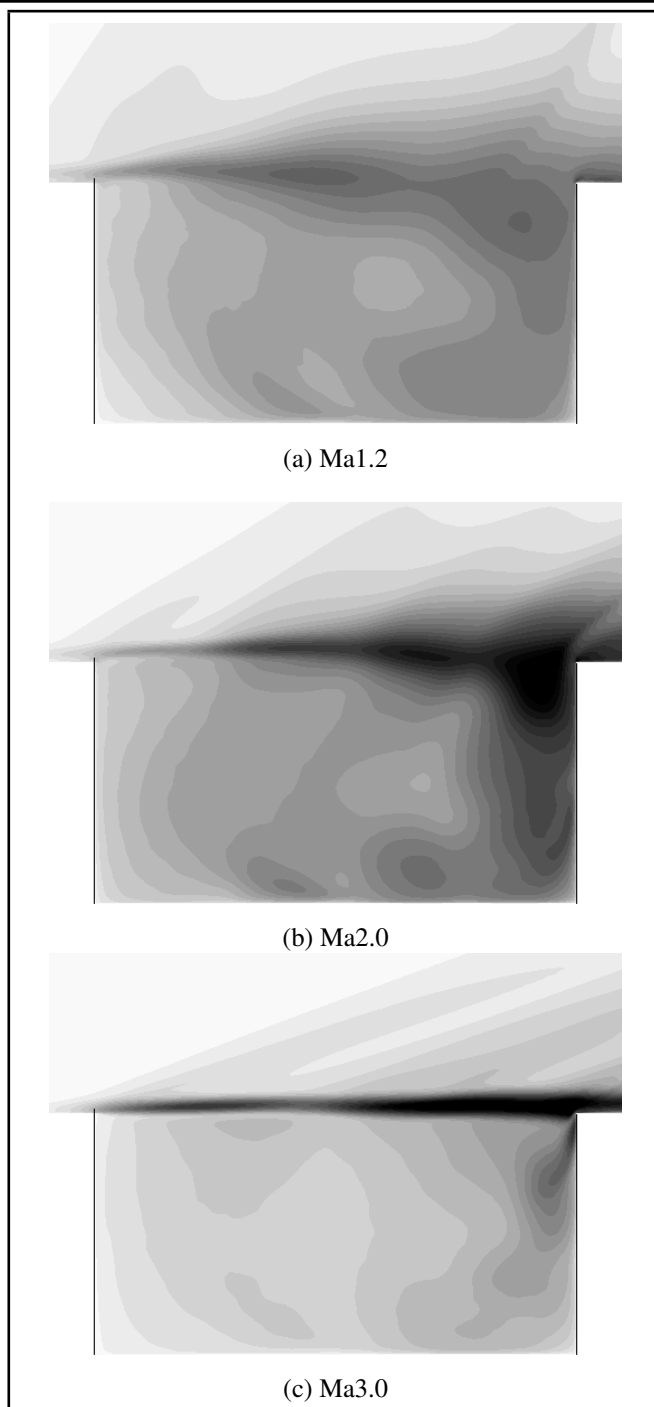

(a) Ma1.2

(b) Ma2.0

(c) Ma3.0

Figure 7. Contours of turbulence kinetic energy ($0 < TKE < 0.5_\infty a_\infty^2$).

Therefore, we mainly focus on the impinging and passage of vortex S_2. A quadratic polynomial is used to interpolate the convection trajectories of vortex S_2. It showed that the vortex S2 impinges on the trailing edge at a phase angle of approximately $-2/15\pi$, $-2/15\pi$ and $-1/30\pi$ in the Ma1.2, Ma2.0 and Ma3.0 case, respectively. The vortex S_1 in the Ma3.0 case is not shown since it is somehow too flat to be detected. Figure 10 shows pressure oscillations at P_2 (depicted in Fig. 8). The P_2 is selected among several points close to the trailing-edge lip. All the points have similar variation tendencies but are different in the amplitude of the pressure.

In Fig. 9 and 10 the lowest pressure values occur when the cores of the vortex S_2 impinges on the cavity trailing-edge lip, and the lowest pressure values are smaller than the freestream
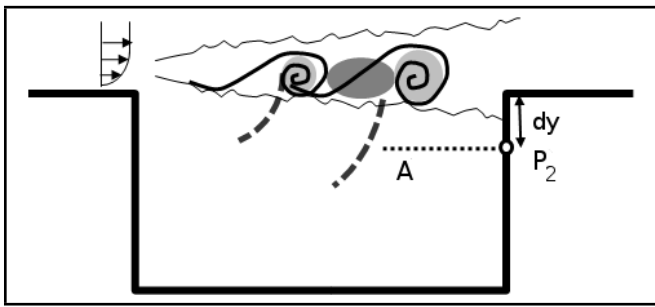
Figure 8. Schematic of large-scale vortices and Mach waves.

pressure. It indicates that the pressure decreasing is related to the vortices impingement. After the core of the vortex S_2 passes over the cavity, the pressure value begins to increase. The feedback compression wave is generated when the large-scale vortices passes over the trailing edge, rather than when they impinge on the trailing edge.

A more physical explanation is given here. Before the vortices impingement low pressure values are associated with the cores of the vortices.[26,27] The pressure gradient near the vortices cores is balanced with the centrifugal force of large-scale vortices. When the large-scale vortices impinge on the trailing edge, large velocity distortions and deformations are produced. The balance between the pressure gradient and the centrifugal force of vortices is broken up. The low pressure values are consequently no longer associated with the large-scale vortices and begin to spread near the aft wall. After the vortices impingement the pressure begins to increase since a stagnation region exists in the adjacent point of two neighbor vortices. In summary, the successive passage of large-scale vortices over the cavity trailing edge, which are associated with periodic vorticity productions and pressure pulses near the cavity trailing-edge lip, results in the generation of acoustic disturbances represented by internal upstream-traveling compression waves.

4.2. Reflection of Mach Waves

Figures 11 and 12 are plotted to reveal that the reflection of Mach waves occurs in the Ma2.0 and Ma3.0 cases. Phases-averaged flow fields are used. The background contours are the divergence of velocity ($-2 < div\mathbf{u} < -0.1$), and black contour lines represent the second-order invariant of velocity gradient tensors ($2(a_\infty/D)^2 < Q_{2nd} < 20(a_\infty/D)^2$). Following the definition in Li et al., the Mach wave and feedback (upstream-travelling) compression wave are named as III and IV, respectively.[24] As shown in Fig. 11(a), a Mach wave III propagates downstream associated with the vortex S_2. As time passes, the Mach wave III encounters the cavity aft wall, and a small part of it is reflected off the aft wall, as illustrated in Fig. 11(b). Point R is the reflection position. This reflection procedure continues as long as the Mach wave travels downstream. In Fig. 11(c), an upstream-traveling feedback compression wave IV is generated near the cavity trailing edge. Figure 11(d) shows that a large part of the Mach wave III has been reflected off the aft wall, and the feedback compression wave IV is leaving the aft wall. Similar results are shown in Fig.12 for the Ma3.0 case. This phenomenon is not observed in the Ma1.2 case since no Mach wave is radiated.

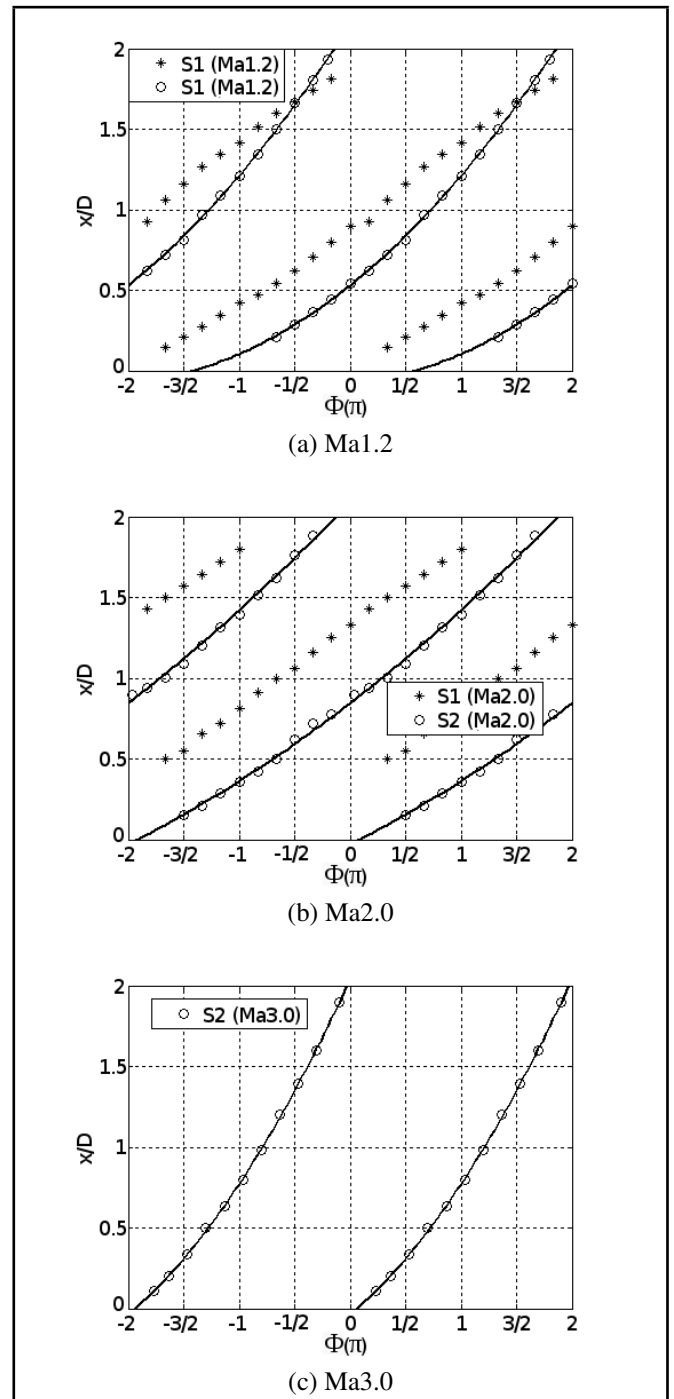Figure 13 shows the propagation of compression waves

(a) Ma1.2

(b) Ma2.0

(c) Ma3.0

Figure 9. Convection trajectories of vortices in streamwise direction.

through Line A (depicted in Fig. 8). The x-coordinates are the streamwise distances, and the y-coordinates represent phase angles. The contours in Fig. 13 are the variations of $div\mathbf{u}$ along Line A. Roughly, the angle α and β can indicate the streamwise velocity of the Mach wave propagating toward the aft wall and the feedback compression wave propagating against the aft wall, respectively. Based on the $x - t$ diagrams in Fig. 13(b) and Fig. 13(c), it is indicates that the phase lag between the Mach wave reaching the aft wall and the feedback compression wave leaving the aft wall are very small. It can be concluded that the reflection of Mach wave is one important factor for the generation of acoustic disturbances in the Ma2.0 and Ma3.0 cases. However, it is not the only reason because the feedback compression waves have higher strength than the
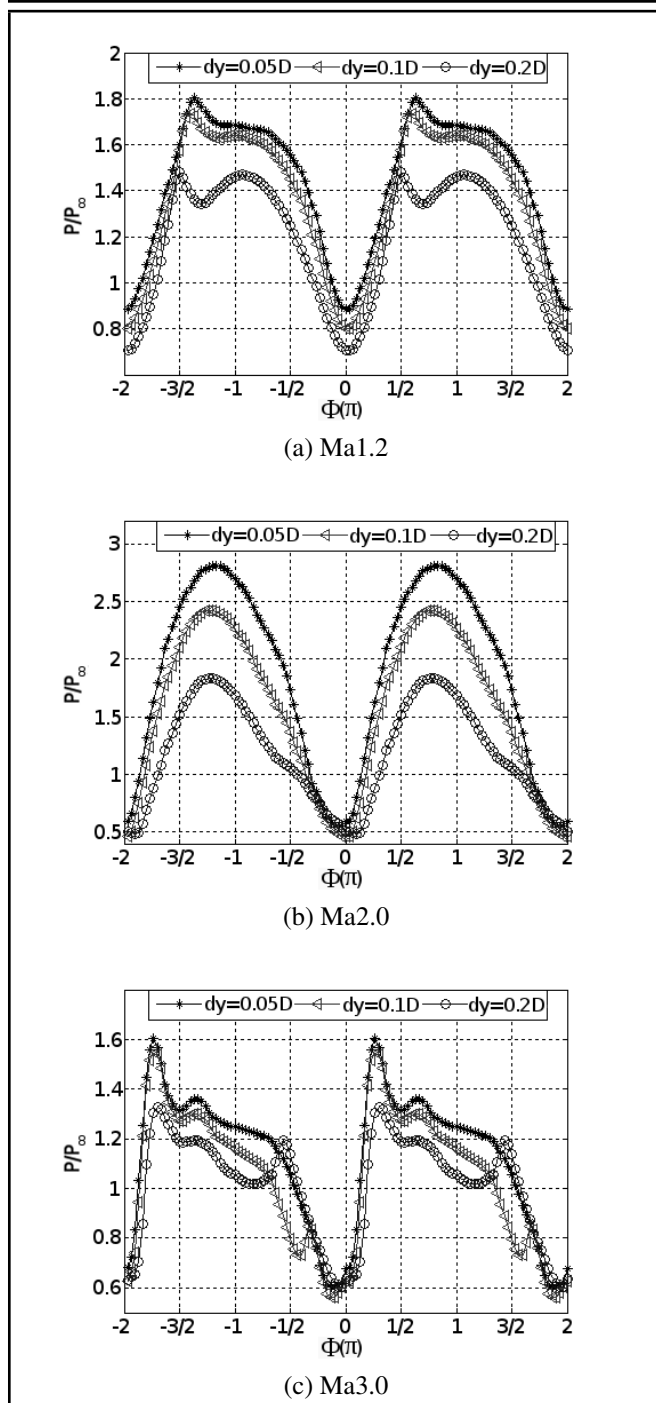
(a) Ma1.2

(b) Ma2.0

(c) Ma3.0

Figure 10. Pressure oscillations at P_2.

Mach waves, and no Mach wave is radiated in the Ma1.2 case in which strong self-sustained oscillations are also exhibited.

It is difficult to distinguish the action caused by the passage of large-scale vortices and the reflection of Mach wave in the Ma2.0 and Ma3.0 cases. In the Appendix, a two-dimensional simulation of a laminar free shear layer subjected to an artificial acoustic source is performed. Results suggest that the successive passage of large-scale vortices over the tailing edge is the dominant reason for the generation of acoustic disturbances, but the Mach waves could significantly enhance the strength of the acoustic disturbances and cavity instabilities. In engineering and presumably in other fields, controlling the upstream laminar flow by facilitating shear-layer three-dimensionality would be desirable in order to suppress the con-

tributions of Mach waves and reduce the pressure oscillations inside the cavity.

5. CONCLUSIONS

Supersonic laminar flows ($M = 1.2/2.0/3.0$ and $Re_D = 10^5$) past a rectangular cavity ($L/D = 2$) are studied with high-resolution implicit large-eddy simulations. Results show that a transition procedure from laminar inflow to turbulence exists near the leading edge of the cavity before the shear layer resumes a linear growth rate. Compressibility effects have significant impacts on the shear-layer development and fluctuation properties. Two mechanisms are addressed for the generation of acoustic disturbances in supersonic laminar cavity flows. First, the successive passage of large-scale vortices over the cavity trailing edge, associated with periodical vorticity productions and pressure pulses, is the dominant reason for the acoustic radiation in the vicinity of the cavity trailing edge. Secondly, Mach waves may be radiated from the cavity shear layer once the large-scale vortices convect at supersonic speed with respect to the sound speed of surrounding streams. The reflection of Mach waves could take place at the cavity aft wall and have large contributions for the acoustic radiation in terms of enhancing the strength of the feedback compression waves.

REFERENCES

[1] Grace, S. M. An Overview of Computational Aeroacoustic Techniques Applied to Cavity Noise Prediction, *AIAA Paper* 2001-0510.

[2] Colonius, T. An Overview of Simulation, Modeling, and Active Control of Flow/acoustic Resonance in Open Cavities, *AIAA Paper 2001-0076*, (2001).

[3] Zhuang, N. Alvi, F. S., Alkislar, M. B., and Shih, C. Supersonic Cavity Flows and Their Control, *AIAA Journal*, **44**(9), 2118–2128, (2006).

[4] Rockwell, D. and Naudascher, E. Review: Self-Sustaining Oscillations of Flow Past Cavities, *Journal of Fluids Engineering*, **100**(2), 152–165, (1978).

[5] Lawson, S. J. and Barakos, G. N. Review of Numerical Simulations for High-speed, Turbulent Cavity Flows, *Progress in Aerospace Science*, **47**(3), 186–216, (2011).

[6] Powell, A. On the Edge Tone, *Journal of the Acoustical Society of America*, **33**(395), 395–409, (1961).

[7] Rossiter, J. E. Wind-Tunnel Experiments on the Flow over Rectangular Cavities at Subsonic and Transonic Speeds, *Aeronautical Research Council Reports and Memoranda*, 3438, (1964).

[8] Heller, H. H., Holmes, G., and Covert, E. Flow-induced Pressure Oscillations in Shallow Cavities, AFFDL TR-70-104.

[9] Heller, H. H. and Bliss, D. B. The Physical Mechanism of Flow-induced Pressure in Cavities and Concepts for Their Suppression, AIAA Paper 1975–491.
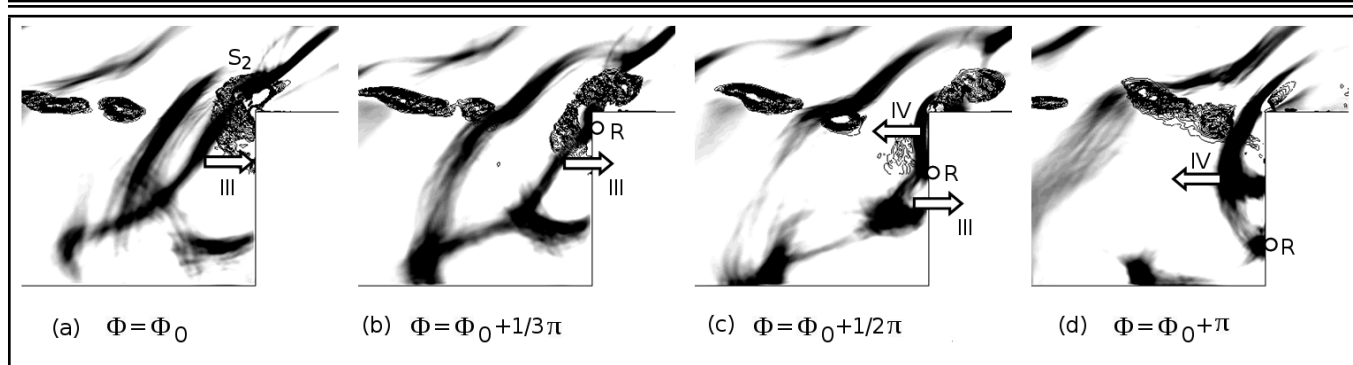
Figure 11. Reflection of Mach waves in Ma2.0 case. Background contours represent the divergence of velocity ($-2 < div\mathbf{u} < -0.1$), and black contour lines represent the second-order invariant of velocity gradient tensors ($2(a_\infty/D)^2 < Q_{2nd} < 20(a_\infty/D)^2$).
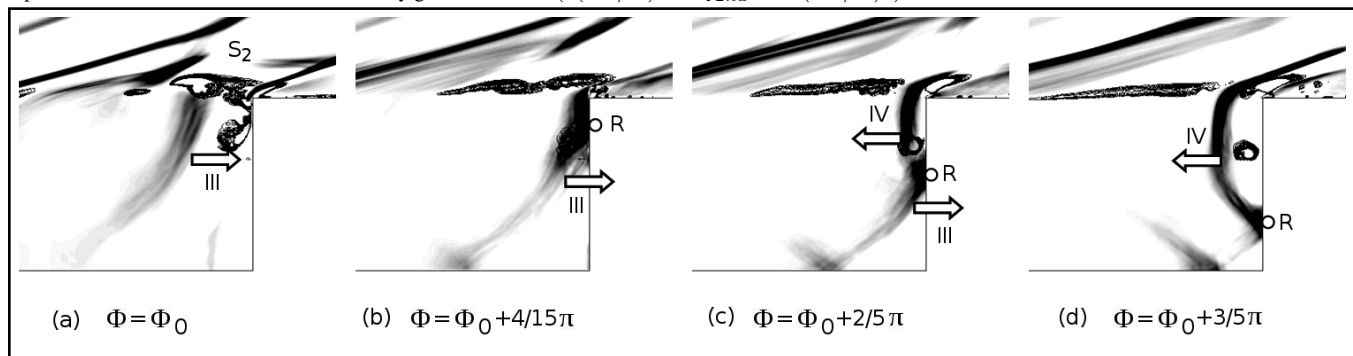

Figure 12. Reflection of Mach waves in the Ma3.0 case. Background contours represent the divergence of velocity ($-2 < div\mathbf{u} < -0.1$), and black contour lines represent the second-order invariant of velocity gradient tensors ($2(a_\infty/D)^2 < Q_{2nd} < 20(a_\infty/D)^2$).
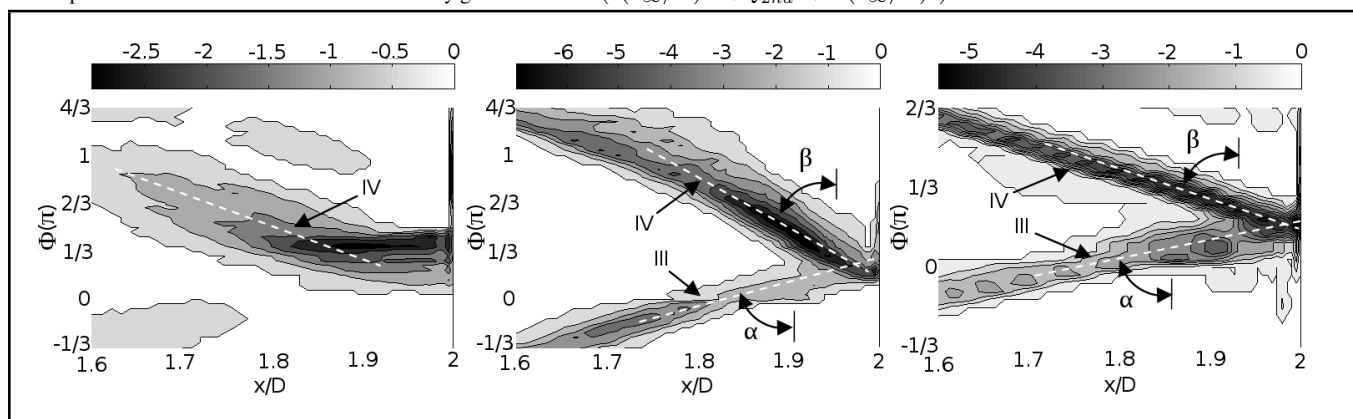

Figure 13. $x - t$ diagrams of compression wave propagating through Line A.

[10] Zhang, X. Compressible Cavity Flow Oscillation due to Shear-layer Instabilities and Pressure Feedback, *AIAA Journal*, **33**(8), 1404–1411, (1995).

[11] Tam, C. J., Orkwis, P. D., and Disimile, P. J. Supersonic Open Cavity Flow Physics Ascertained from Algebraic Turbulence Model Simulations, AIAA Paper 1996–0075.

[12] Schmit, R. F., Semmelmayer, F., Haverkamp, M., and Grove, J. E. Fourier Analysis of High Speed Shadowgraph Images around a Mach 1.5 Cavity Flow Field, AIAA 2011–3961.

[13] Krishnamurty, K. Acoustic Radiation from Two-dimensional Rectangular Cutouts in Aerodynamic Surfaces,Tech. Rep., NACA-TN-3487, 1955.

[14] Heller, H. H., Holmes, D. G., and Covert, E. E. Flow-Induced Pressure Oscillations in Shallow Cavities, *Journal of Sound and Vibration*, **18**(4), 545–553, (1971).

[15] Gloerfelt, X., Bogey, C., Baillyand, C., Juvé, D. Aerodynamic Noise Induced by Laminar and Turbulent Boundary Layers over Rectangular Cavities, AIAA 2002–247.

[16] Nonomura, T. and Fujii, K. Effects of Difference Scheme Type in High-order Weighted Compact Nonlinear Schemes, *Journal of Computational Physics*, **228**, 3533–3539, (2009).

[17] Nonomura, T., Iizuka, N., and Fujii, K. Freestream and Vortex Preservation Properties of High-order WENO and WCNS on Curvilinear Grids, *Computers and Fluids*, **39**, 197–214, (2010).

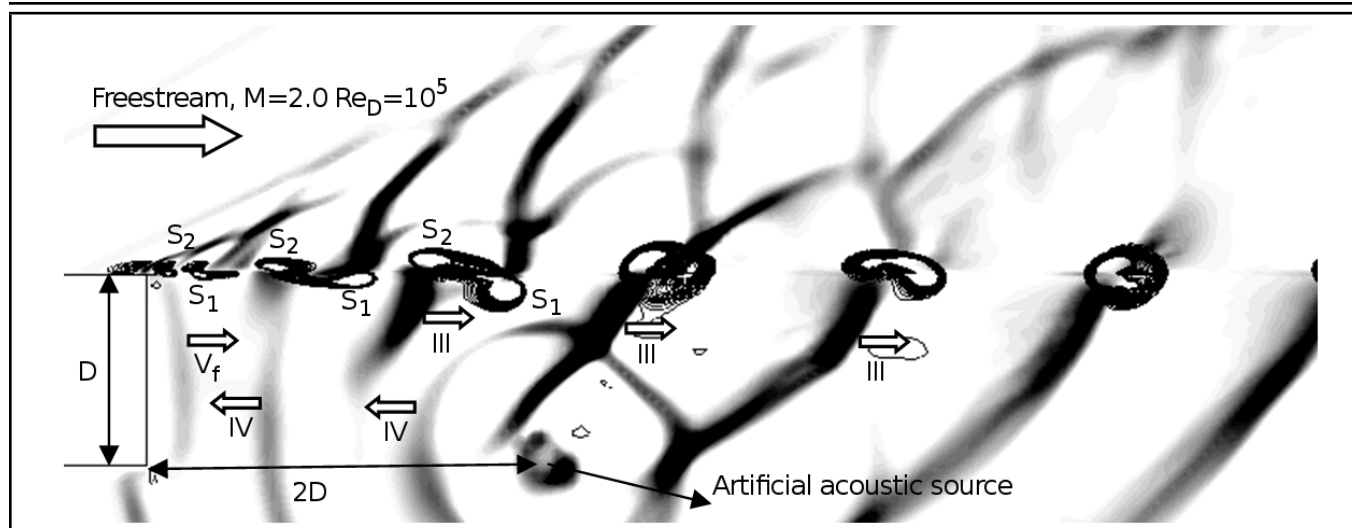[18] Nonomura, T., Li, W., Goto, Y., and Fujii, K. Efficiency Im-

Figure A1. Free shear-layer subjected to an artificial acoustic source. Background contours represent the divergence of velocity ($-2 < div\mathbf{u} < -0.1$), and black contour lines represent the second-order invariant of velocity gradient tensors ($(a_\infty/D)^2 < Q_{2nd} < 15(a_\infty/D)^2$).

provements of Seventh-order Weighted Compact Nonlinear Scheme, *CFD Journal*, **18**(2), 193–198, (2010).

[19] Shima, E. and Jounouchi, T. Role of CFD in Aeronautical Engineering (No. 14) -AUSM type Upwind Schemes, *Proceedings of the 14th NAL Symposium on Aircraft Computational Aerodynamics*, National Aeroautical Laboratory, 7–12, (1997).

[20] Nishida, H. and Nonomura, T. ADI-SGS Scheme on Ideal Magnetohydrodynamics, *Journal of Computational Physics*, **228**, 3182–3188, (2009).

[21] Zhuang, N., Alvi, F. S., and Shih, S. Another Look at Supersonic Cavity Flows and Their Control, AIAA Paper 2005–2803.

[22] Forestier, N., Jacquin, L., and Geffroy, P. The Mixing Layer over a Deep Cavity at High-subsonic Speed, *Journal of Fluid Mechanics*, **475**, 101–145, (2003).

[23] Sandham, N. D. and Reynolds, W. C. Compressible Mixing Layer: Linear Theory and Direct Simulation, *AIAA Journal*, **18**(4), 618–624, (1990).

[24] Li, W., Nonomura, T., Oyamaand, A., and Fujii, K. Feedback Mechanism in Supersonic Laminar Cavity Flows, *AIAA Journal*, **51**(1), 253–257, (2013).

[25] Larchevêque, L., Sagaut, P., Maryand, I., Labbé, O. Large-eddy Simulation of a Compressible Flow Past a Deep Cavity, *Physic1 of Fluids*, **15**(1), 193–210, (2003).

[26] Lele, S. K. Direct Numerical Simulation of Compressible Free Shear Flows, AIAA1989-0374.

[27] Robinson, S. K. Coherent Motions in the Turbulent Boundary Layer, *Annual Review of Fluid Mechanics*, **23**, 601–639, (1991).

[28] Yokoyama, H. and Kato, C. Fluid-acoustic Interactions in Self-sustained Oscillations in Turbulent Cavity Flows. I. Fluid-dynamic Oscillations, *Physics of Fluids*, **21**, 105103, (2009).

APPENDIX

A two-dimensional simulation of laminar free shear layer subjected to an artificial acoustic source was conducted. The aft wall and bottom wall of the cavity were removed. The flow conditions were the same as the Ma2.0 case. The artificial acoustic source locateed at the same position of the cavity's right bottom corner. Its definition follows Eqs. (16)-(18) described in Lele's work.[26] The non-dimensional amplitude A/∞ are 3.0×10^{-5}, and the frequency f is the same as the dominant frequency for the cavity flow.

Figure A1 shows a scenario of phase-averaged flow-fields. The background contours represent the divergence of velocity, and black contour lines represent the second-order invariant of velocitygradient tensors. Wave IV represents the compression waves radiated from the artificial acoustic source; III represents the Mach waves; V_f represents the front-wall reflection waves. Similar to the cavity flow, two vortices S_1 and S_2 roll up from the leading edge periodically in the phase of each acoustic excitation caused by the compression waves radiated from the artificial acoustic source. The scales of vortices are amplified by Kelvin-Helmholtz instability. Vortex pairing occurs downstream.

The Mach waves radiated from the shear layer are just beneath the large-scale vortices. Assuming that a cavity aft wall is located downstream, when the large-scale vortical structures impinge on the cavity aft wall, it is surely followed by an action of the reflection of Mach waves. Since the radiation of Mach waves is essentially caused by the convection of large-scale vortices, it is desirable to state that the dominant reason for the generation of acoustic disturbances in supersonic laminar cavity flows is the successive passage of large-scale vortices over the trailing edge.